Conference or Workshop Item:
Brisset, Alexandra Helene Marie Brigitte orcid.org/0000-0003-3217-1106, Bieniek, M, Invernizzi, Laurent et al. (3 more authors) (2022) Production of radicals in a He+H2O nanosecond pulsed high-voltage plasma, experimental and numerical analysis. In: Gaseous Electronics Conference, 03-07 Oct 2022.

O and H production in a He+H_2O nanosecond pulsed high-voltage plasma, probed with ps-TALIF Kinetics study using 1D fluid modelling

[1]A. Brisset, [2]M. Bieniek, [1]L. Invernizzi, [1]J. Walsh, [2]M. Hasan, [1]E. Wagenaars

[1]York Plasma Institute, Department of Physics, University of York, York, YO10 5DD, UK
[2]Department of Electrical Engineering and Electronics, University of Liverpool, Merseyside,UK

Summary:

The spatial and temporal evolution of the density of atomic oxygen and hydrogen in a pin-to-pin atmospheric pressure plasma are measured using the Two-photon Absorption Laser Induced Fluorescence (TALIF) diagnostic with a picosecond excitation and detection system. These measurements are carried out in a mixture of 1 slm helium and 0.1%-0.25% water. The plasma is generated by tailored ns-voltage pulses (voltage rise rate ~80 V.ns^{-1}). A 1D fluid numerical model is validated and used to study the kinetics of O and H in the discharge.

Introduction:

In biomedicine, the emphasis is currently on understanding and optimizing the production of O-, H- and N-species that have a high oxidative power and play major roles in biological functions [1]. The tailoring of atmospheric pressure plasmas is complicated by the high gas collisionality leading to fast relaxation and quenching processes. It is therefore usually achieved by adjusting external parameters such as: the gas composition, the electric field distribution (by modifying the source design), or the applied voltage characteristics. This work focuses on atmospheric pressure plasmas generated in a pin-to-pin configuration with a high-voltage ns pulse in varying gas compositions to estimate the range of control offered on radicals production.

Experimental setup:

- Pin-pin geometry, 2.2 mm gap
- ~ 500µm pin radius
- Voltage peaks at 2 kV
- Repetition frequency: 5 kHz
- P = 1 atm, 1 L.min^{-1} flow of humid He

- Nd:YAG pulsed laser (100µJ – 32ps – 5 kHz)
- ICCD Stanford Computer Optics 4-Picos
- Variable attenuators CaF_2

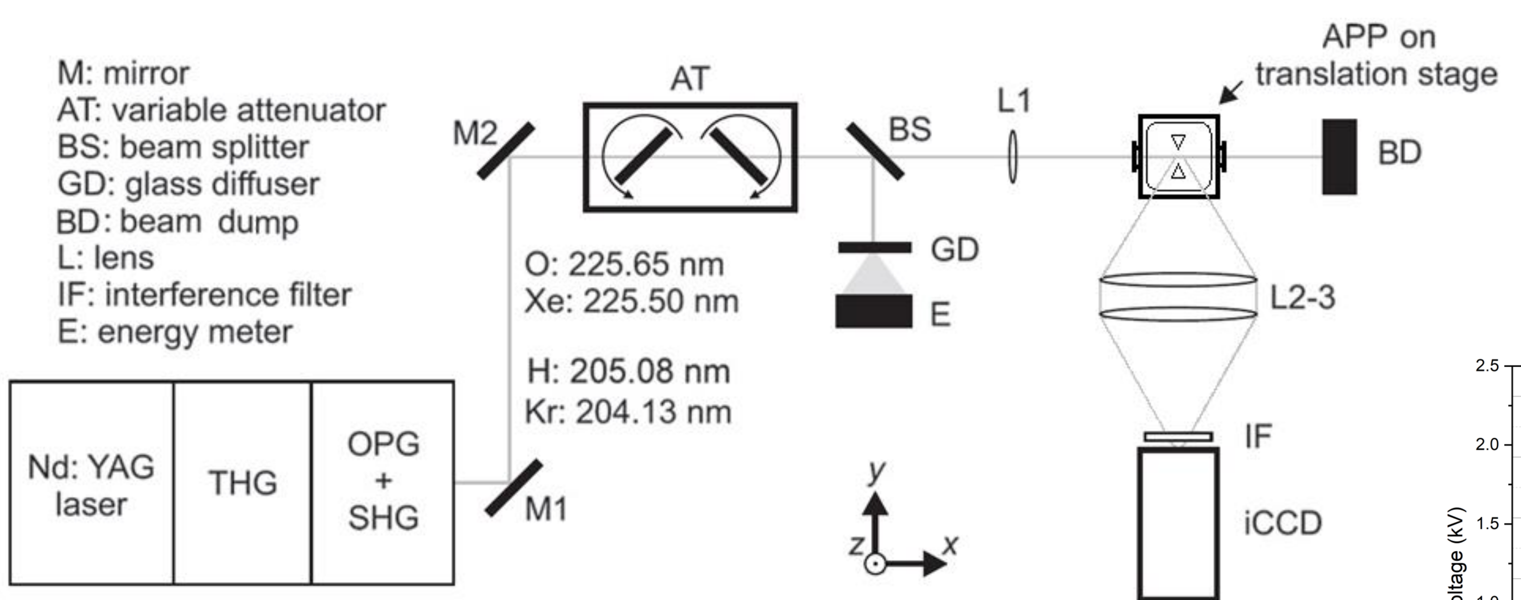

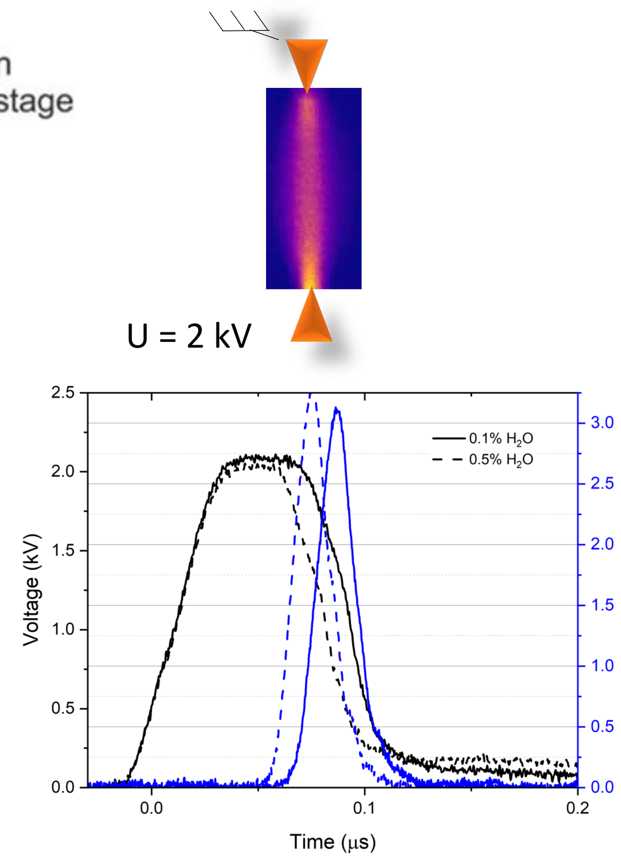

A home-made high-voltage switch box connected to a DC-power supply generates the **nanosecond voltage pulses** at a frequency of **5 kHz** with adjustable rise and fall times.

For each studied condition, the **energy of the discharge is kept constant** by adjusting the voltage amplitude.

The **laser pulse energy** is controlled over time with a pair of variable attenuators coupled to an energy meter. At every laser shot, the energy is monitored and compared to the target energy value and the pair of attenuators is rotated accordingly by a stepper motor to increase or lower the laser beam energy of the next shot. Scheme and method adapted from [2]

TALIF in the non-saturated regime using the well-known noble-gas calibration technique :

In this regime, the density of the excited state probed species n_x is related to the density of the gas used for calibration n_{cal} through:

$$\frac{S_{F,x}}{S_{F,cal}} = \frac{\eta(\lambda_{F,x})}{\eta(\lambda_{F,cal})}\frac{T_f(\lambda_{F,x})}{T_f(\lambda_{F,cal})}\frac{T_w(\lambda_{F,x})}{T_c(\lambda_{F,cal})}\frac{a_{ik,x}}{a_{ik,cal}}\frac{\sigma_x^{(2)}}{\sigma_{cal}^{(2)}}\frac{\boldsymbol{n_x}}{n_{cal}}\left(\frac{E_x}{E_{cal}}\frac{\lambda_{L,x}}{\lambda_{L,cal}}\right)^2$$

S_F: measured fluorescence signal, integrated spatially, temporally and spectrally,

$\eta(\lambda_F)$: camera quantum efficiency at the fluorescence wavelength λ_F,

$T_{f/w/c}$: transmission coefficients of the filter/reactor window/cuvette wall,

a_{ik}: branching ratios of the transitions ($a_{ik} = \frac{A_{ik}}{\sum_k A_{ik} + \sum_q k_q^i n_q}$, where A_{ik} is the Einstein coefficient of the transition from state i to k, k_q^i is the quenching rate between species q and i),

$\sigma^{(2)}$: cross sections for two-photon absorption,

E: laser energy at the position of TALIF measurement

λ_L: laser wavelength

Ps-decay time measurement:

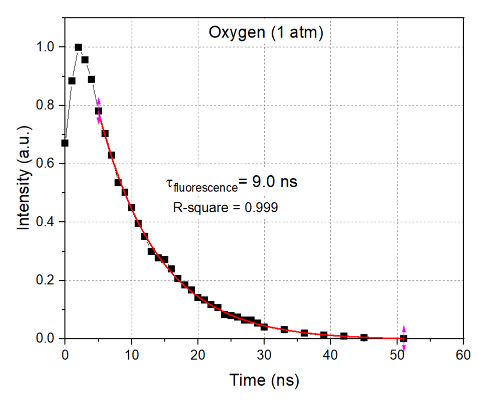

Measured fluorescence decay for O(3p ^{3}P) - 1 slm He, 0.1%H_2O

Since the camera gate widths are larger than the respective gate steps, the measured signals overlap temporally. But the choice of gate step (0.2 to 3 ns) and width (5 to 10 ns) does not affect the measured lifetimes.

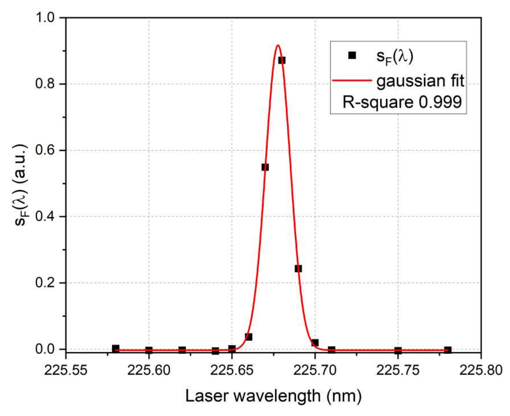

Wavelength scan of fluorescence signal integrated over x, t for O

S_F is the area of the Gaussian function that best fits the wavelength profile $s(\lambda)$. Its width is dominated by the laser line profile (4 cm^{-1} - 20 pm).

Non-saturated regime:

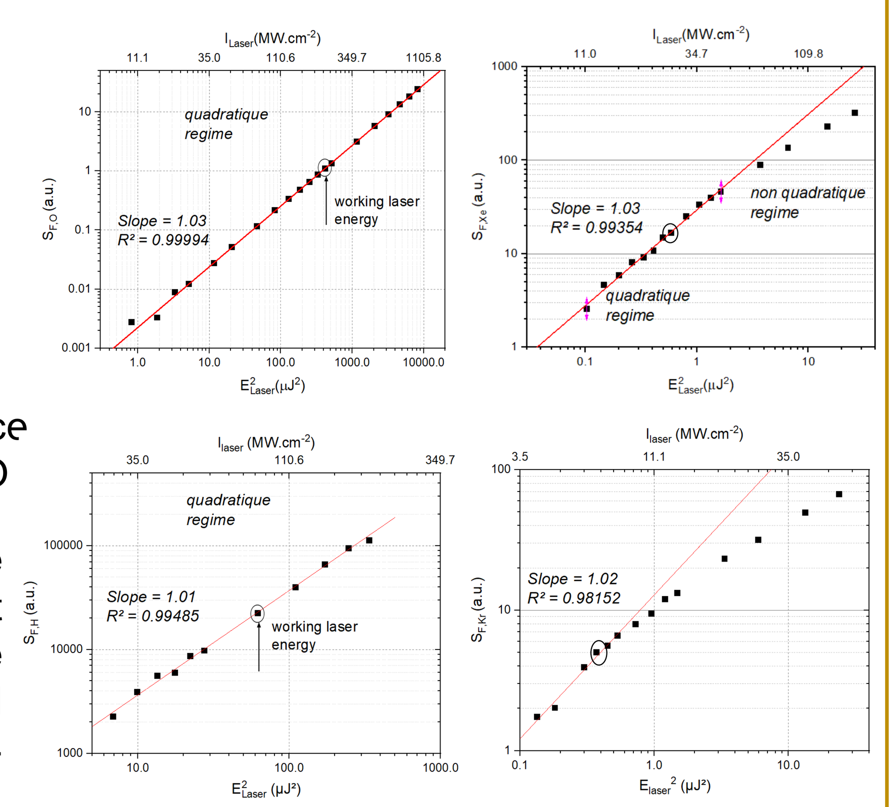

Axial profiles for O at 4 µs:

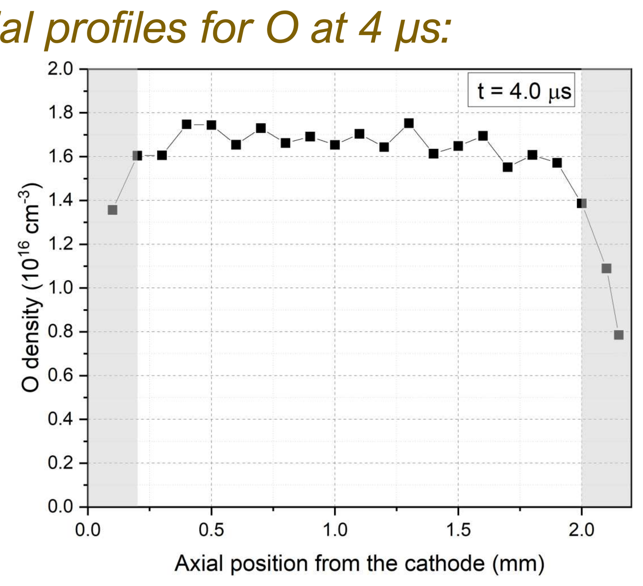

- **Axial O density profile is constant** within experimental uncertainty.
- The grey areas are impacted by loss of TALIF signal by interaction with the electrodes (Ω, beam truncation).

Temporal evolution of O and H densities (exp. and sim.) at mid gap at 1 slm He + (0.1 / 0.25%) H_2O:

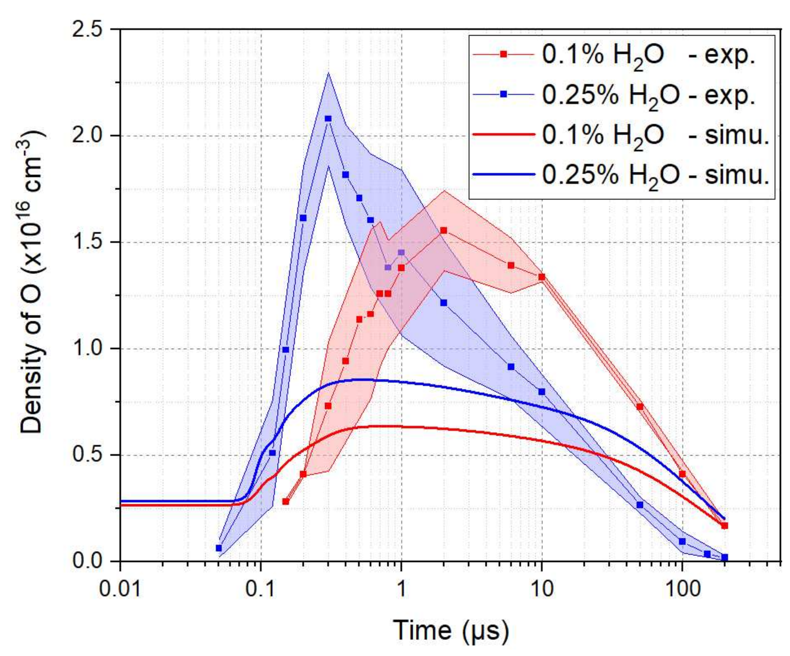

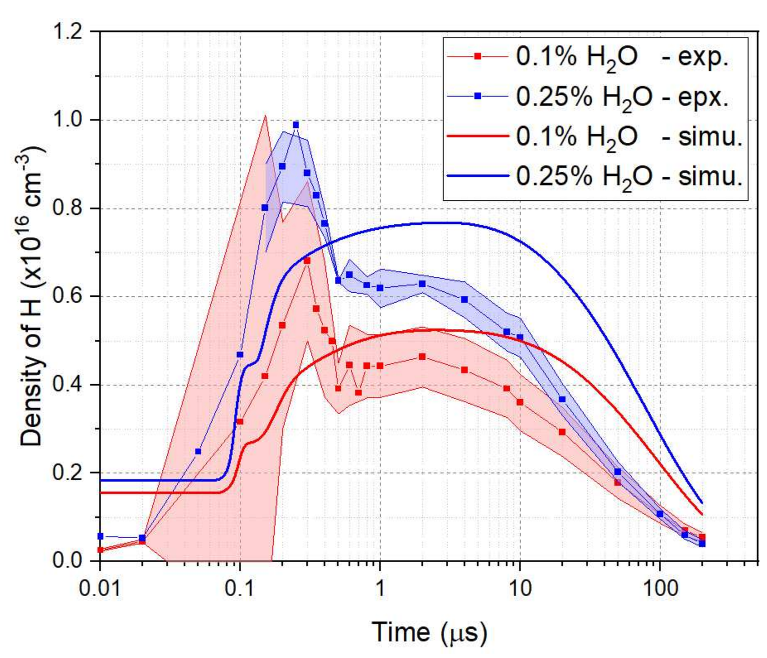

- Agreement within a factor ~2 between experiment and simulation
- Enhanced production of O during the pulse at increased water vapour concentrations reproduced by the model
- Production of H during the discharge phase underestimated by the model
- Losses in the afterglow underestimated by the model. Radial losses are included using a loss rate D/R^2 (D: diffusion coefficient - R: characteristic length of the gradient of species number density)

Note : Model run for 3 pulses (steady state not reached)

Model description:

- Common 1D plasma fluid model similar to [3]
- Uses the local mean energy approximation
- Electron transport and reaction coefficients use the solution of the local steady state two-term Boltzmann equation
- Boundary conditions at the anode: absorbing of a thermal flux of plasma species, inducing of electron density, and condition for pulses of the applied voltage
- Secondary emission coefficient, γ, set to 0.15
- Work function of cathode material set to 4.08eV
- O_2 initial density is difficult to estimate. Production of O by electron impact dissociation of O_2 is still dominant for low initial concentrations of O_2 (<0.001%) at 0.1%H_2O. Initial O_2 density used: 200 ppm.

Production and loss pathways of O and H at 0.1%H_2O:

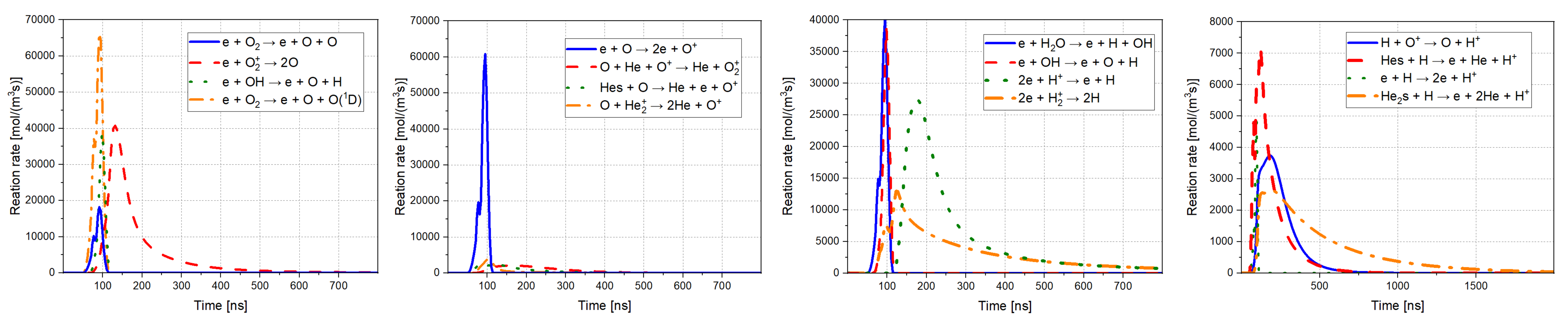

O production:
- **t <100ns**: electron impact dissociation of O_2 and OH
- **t >100ns**: dissociative recombination of O_2^+ with e
- **t >300ns**: O production is small

O losses:
- **t <100ns**: O ionisation by electron impact and charge exchange with He_2^+
- **t >100ns**: 3-body formation of O_2^+ with He as 3rd body
- The model does not yet resolve potential kinetic losses in the afterglow

H production:
- **t <100ns:** dissociation of H_2O and OH by electron impact
- **t >100ns**: 3-body recombination of H^+ and H_2^+ with e^-

H losses:
- **t <100 ns**: Ionisation by e^-, He^*
- **t >100 ns**: charge exchange with O^+ dominantly and ionisation by He_2^* over the first microsecond.

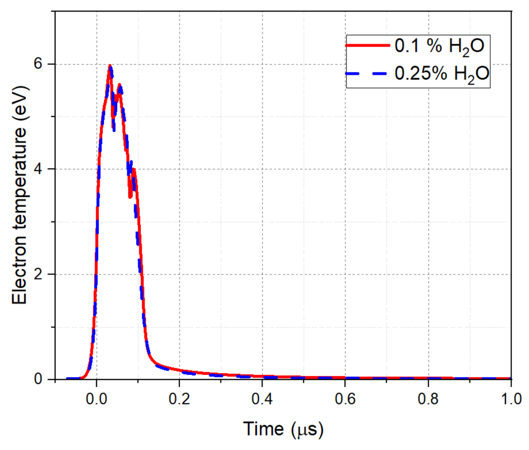

Electron properties in He+H_2O (modelling):

- T_e ~ 6 eV during the discharge and relaxes to <0.5 eV in about 100 ns – Induces :
  - electron impact dissociation during the discharge
  - dissociative recombination during the early and late afterglow
- Peak n_e ~ 5x10^{21} m^{-3}

Conclusion:

Results of the 1D numerical model agree reasonably well with absolute peak density of O and H obtained by ps-TALIF. Long term loss mechanisms need to be refined (radial diffusion, refined kinetics, gas flow refreshment). Non-equilibrium high voltage ns-pulsed He+H_2O discharge in the low density mode produce O and H radicals mostly by electron impact dissociation and dissociative recombination and losses are mostly due to ionisation and 3-body recombination processes.

Acknowledgments: This work is supported by EP/S026584/1 and EP/S025790/1 research programs.

References:

[1] Brisset et al., J. Phys. D: Appl. Phys. 54 285201 (2021)
[2] Schröter Plasma Sources Sci. Technol. 29 (2020) 105001
[3] M. S. Bieniek et al, Physics of Plasmas, 25, (2018)